ISA Transactions 140 (2023) 32–45

Contents lists available at ScienceDirect

ISA Transactions

journal homepage: www.elsevier.com/locate/isatrans

Research article

Observer-based H_∞ fuzzy fault-tolerant switching control for ship course tracking with steering machine fault detection

Xuelin Zhang [a,b], Xiaobin Xu [a,b], Jianning Li [b,*], Yang Luo [c], Guodong Wang [d], Georg Brunauer [e], Schahram Dustdar [f]

[a] China-Austria Belt and Road Joint Laboratory on Artificial Intelligence and Advanced Manufacturing, Hangzhou Dianzi University, Hangzhou 310018, China
[b] School of Automation, Hangzhou Dianzi University, Hangzhou 310018, Zhejiang, China
[c] Hangzhou Qianhang Shipyard Co., LTD, Hangzhou 311256, Zhejiang, China
[d] Sino-Austria Research Institute for Intelligent Industries (Nanjing) Co.,Ltd., Nanjing 210003, China
[e] TU Wien, Institute for Energy Systems and Thermodynamics, Getreidemarkt 9, 1060 Vienna, Austria
[f] Distributed Systems Group, TU Wien, 1040 Vienna, Austria

A R T I C L E I N F O

Article history:
Received 28 February 2023
Received in revised form 27 May 2023
Accepted 28 May 2023
Available online 31 May 2023

Keywords:
Takagi–Sugeno fuzzy nonlinear ship autopilot
Steering machine fault
Fault-tolerant control
Virtual fuzzy observer
Fault detection and alarm
Smoothed Z-score algorithm

A B S T R A C T

To enhance the robustness of ship autopilot (SA) system with nonlinear dynamics, unmeasured states, and unknown steering machine fault, an observer-based H_∞ fuzzy fault-tolerant switching control for ship course tracking is proposed. Firstly, a global Takagi–Sugeno (T-S) fuzzy nonlinear ship autopilot (NSA) is developed with full consideration of ship steering characteristics. And the actual navigation data collected from a real ship are used to verify the reasonableness and feasibility of NSA model. Then, virtual fuzzy observers (VFOs) for both fault-free and faulty systems are proposed to estimate the unmeasured states and unknown fault simultaneously, and compensate for the faulty system by using the fault estimates. Accordingly, the VFO-based H_∞ robust controller (VFO-HRC) and fault-tolerant controller (VFO-HFTC) are designed. Subsequently, a smoothed Z-score-based fault detection and alarm (FDA) is developed to provide switching signals for which the controller and its corresponding observer should be invoked. Finally, simulation results on the "Yulong" ship demonstrate the effectiveness of the developed control method.

1. Introduction

As a critical device for ship navigation, SA can automatically maneuver the steering machine according to the predetermined control requirements, which enables the ship to navigate autonomously [1]. Since the PID control algorithm was applied to SA control [2], the autopilot has received attention for its advantages of safe navigation, energy saving, and lowering the working intensity of crew. The steering machine, as an important actuator of SA system, controls the adjustment and modification of ship's heading. Moreover, its healthy state has a significant influence on the stability of heading control and ship navigation safety [3]. During ship navigation, the steering machine is susceptible to failures caused by the coupling between its component units [4]. At this time, the SA system will not be controlled effectively due to the influence of steering machine fault, which causes the ship to yaw and affects navigation safety. Consequently, it is necessary to establish a high-performance course tracking control system with an advanced control strategy to ensure that SA system can operate efficiently, safely, and reliably in faulty situations, and to further ensure the safe navigation of the ship.

Concerning SA system, there are mainly two types of controllers, including linear controllers and non-linear controllers. For linear controller design, the linear model (e.g., Nomoto model) that describes the steering characteristics of a ship is widely used in the design of ship course-keeping autopilots due to its compromise between simplicity and accuracy [5–9]. The linear model-based controller can meet the requirements of ship motion in course-keeping situations. However, during the ship navigation, the ship may be required to perform course changing motion according to the actual navigation environment or work allocation assignment requirements. At this time, the ship motion involves large-scale steering and presents serious nonlinear characteristics. The linear model-based controller will be inadequate for course changing maneuvers. Consequently, various excellent control approaches related to course changing control have been developed [10–13]. Specifically, based on the Hurwitz condition, a non-linear controller was devised by Perera et al. [10] to fulfill the course-keeping and course changing maneuvering during the ship

* Corresponding author.
E-mail address: ljn@hdu.edu.cn (J. Li).

https://doi.org/10.1016/j.isatra.2023.05.021

navigation. In [11], an adaptive course tracking control method was proposed, which fully considered the characteristics of SA system model with parameter uncertainty and unknown external disturbances. The course tracking problem of surface ships was investigated and an adaptive backward controller was proposed by Liu and Chu [12] and Liu [13]. To the best of the authors' knowledge, Zhang and Yang et al. [14–22] have made intensive research and significant contributions for SA control.

All the work mentioned above did not consider the effect of steering machine fault on the system performance when designing a course tracking controller. However, the steering machine is subject to failure during the ship navigation due to the coupling effect between its component units. In this case, the conventional robust controller cannot meet the stability requirements of SA system in faulty situations. To this end, Omerdic et al. [23] proposed a heuristic approach in the design of a fault-tolerant control system for ship course tracking. An H_∞ robust fault-tolerant controller for navigation control system was designed by Cheng et al. [24]. A robust model predictive control (MPC) method, based on fault-tolerant control, was developed by Zheng et al. [25] for the course and trajectory tracking with system failures. In these works, the introduction of fault-tolerant control techniques has greatly improved the system's tolerance to faults and enables the benign control of SA systems when the fault occurs. However, the controller was designed by assuming that accurate sensor signals could be observed for all the required system states. In practical engineering, some states are not easily measured or cannot be measured directly. Such an assumption undoubtedly increases the cost of sensors. Moreover, such a controller is not suitable for SA system equipped with low-cost sensors. On the other hand, only the passive fault-tolerant controller design for SA systems has been studied in these works. During ship navigation, steering machine is commonly under normal conditions. It should be noted that the conservativeness of SA system will be increased if the fault-tolerant controller is used in fault-free situations. Consequently, it is urgent to design appropriate observer-based controllers according to different faults and provide a switching control strategy so that the system can invoke the corresponding controller according to the fault type.

Motivated by the aforementioned account, we propose an observer-based H_∞ fuzzy fault-tolerant switching control for ship course tracking. Firstly, a global fuzzy model of NSA system is developed with full consideration of ship steering characteristics, and the reasonableness and feasibility of the global fuzzy model are verified. Then, VFOs are designed for fault-free and faulty systems, respectively. Subsequently, VFO-based H_∞ robust controller (VFO-HRC) and fault-tolerant controller (VFO-HFTC) are designed. Furthermore, a smoothed Z-score-based steering machine fault detection and alarm is proposed to provide switching signals for which the controller and its corresponding observer should be invoked. Finally, simulation experiments are performed to illustrate the effectiveness of the developed control method. The main contributions of this work are elaborated as:

1. A novel fault-tolerant switching control for ship course tracking with steering machine fault and FDA is developed so that the NSA system can be controlled appropriately in faulty and fault-free situations.
2. Based on the actual navigation data collected from a real ship, the feasibility and reasonableness of NSA model are verified. To the best of the authors' knowledge, such work was scarce.
3. VFOs are introduced to estimate the unmeasured states and unknown bias fault simultaneously, and VFO-HRC and VFO-HFTC are designed for fault-free and faulty systems, respectively.

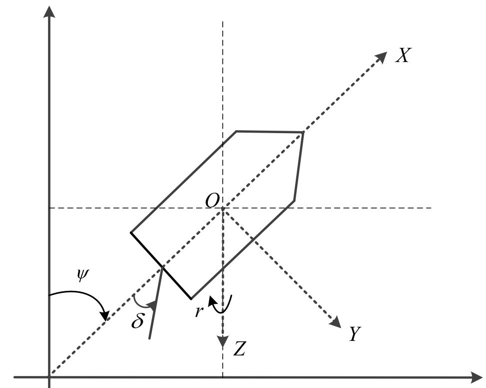

Fig. 1. Ship maneuvering motion coordinate system.

4. A smoothed Z-score-based FDA is designed and the switching signal will be generated for calling the appropriate controller and corresponding observer. Residuals are analyzed for fault detection and alarming, which helps to make the fault more intuitive.

The paper is organized as follows. Section 2 briefly introduces the system modeling of NSA. Section 3 describes the design of H_∞ fuzzy switching control, including VFOs, VFO-HRC, VFO-HFTC, and FDA. Section 4 presents simulation experiments on "Yulong" ship, followed by the conclusions in Section 5.

Notations. $\mathbb{R}^n$ denotes the n-dimensional Euclidean space, while $\mathbb{R}^{n\times m}$ is the real matrix of all $n\times m$. $F > 0$ and $F < 0$ are used to denote that F is positive definite or negative, respectively. $diag\{\cdots\}$ represents a block-diagonal matrix, and $\vartheta \in \mathfrak{L}_2[0,\infty)$ indicates ϑ is energy bounded. F^{-1} is the inverse of a matrix F. F^{T} and $\mathbb{E}\{\bullet\}$ denote the transpose of matrix F and the mathematical expectation, respectively.

2. System modeling and preliminaries

2.1. Modeling and analysis

In Fig. 1, the ship's gravity center (O) is used as the origin and a coordinate system ($OXYZ$) is established to demonstrate the ship maneuvering motion. X, Y, Z, ψ, δ, and $r = \dot{\psi}$ are longitudinal axis, transverse axis, normal axis, actual heading, control rudder angle, and yaw rate, respectively.

For SA design, the linear Nomoto model is generally used to describe the ship maneuvering motion [26]:

$$T\ddot{\psi} + \dot{\psi} = K\delta \tag{1}$$

Normally, Eq. (1) describes the heading dynamics precisely in course-keeping situations. However, in course changing situations, the ship's motion presents serious nonlinear characteristics [11]. The Nomoto model-based linear controller will be inadequate for course changing maneuvers. In this case, the Nomoto model can hardly describe the actual dynamic characteristics of ship accurately. To improve the model description accuracy, based on model derivation and simplification [27], the nonlinear Norrbin model is used to describe the nonlinear maneuvering characteristics of ships.

$$T\ddot{\psi} + \alpha_1\dot{\psi} + \alpha_2\dot{\psi}^2 + \alpha_3\dot{\psi}^3 = K\delta, \tag{2-1}$$

where the nonlinear Norrbin model parameters can be described as $\alpha_i (i = 1, 2, 3)$, Norrbin coefficients; T, time constant; and K, control gain constant. It should be noted that the control rudder angle δ and its change rate $\dot{\delta}$ satisfy $|\delta| \le 35^\circ$ and $|\dot{\delta}| \le 3^\circ/\mathrm{s}$. For a stable ship with symmetrical hull, the Norrbin coefficients satisfy $\alpha_1 = 1$ and $\alpha_2 = 0$. After considering the external disturbances ω, the nonlinear Norrbin model (2-1) can be rewritten as

$$T\ddot{\psi} + \dot{\psi} + \alpha_3\dot{\psi}^3 = K\delta + \omega. \tag{2-2}$$

Remark 1. In actual navigation, the disturbance caused by external environmental factors such as wind, currents, and waves has a significant impact on the stability of ship navigation. Having reviewed the literature in this field, we found that the external environmental disturbance ω was modeled as an uncertainty term in the system model in many studies [6,12,13]. Typically, it is believed that currents are affecting the position of the ship only, which has a negligible effect on the heading [21]. Therefore, it is considered that ω is the wind and waves disturbance.

In this work, the NSA system that consists of Eq. 2-2 is considered. To facilitate the subsequent control design, define the state and control variables $e_1 = \psi_d - \psi$, $e_2 = -\dot{e}_1 + \dot{\psi}_d = \dot{\psi}$, and $u = \delta$. Accordingly, we can get the following expression of NSA system

$$\begin{cases} \dot{e}_1 = -e_2 + \dot{\psi}_d, \\ \dot{e}_2 = -\frac{1}{T}e_2 - \frac{\alpha}{T}e_2^3 + \frac{K}{T}u + \frac{1}{T}\omega, \\ y = -e_1 + \psi_d. \end{cases} \tag{3}$$

From Eq. (3), we have

$$\begin{cases} \dot{e}(t) = f(e(t)) + g(e(t))u(t) + D\varpi(t), \\ y(t) = Ce(t) + \psi_d, \end{cases} \tag{4}$$

where $f(e(t)) = \begin{bmatrix} -e_2 \\ -e_2/T - \alpha e_2^3/T \end{bmatrix}$, $g(e(t)) = \begin{bmatrix} 0 \\ K/T \end{bmatrix}$, $\varpi(t) = \begin{bmatrix} \dot{\psi}_d \\ \omega \end{bmatrix}$, $C = \begin{bmatrix} -1 & 0 \end{bmatrix}$ and $D = \begin{bmatrix} 1 & 0 \\ 0 & 1/T \end{bmatrix}$ are known real constant matrices. ψ_d, $e(t) = [e_1(t), e_2(t)]^{\mathrm{T}}$, $u(t)$ and $y(t)$ represent the desired heading, system state vector, control input, and control output of NSA system, respectively.

Further define the tuned output as $z(t) = Ce(t)$, which yields

$$\begin{cases} \dot{e}(t) = f(e(t)) + g(e(t))u(t) + D\varpi(t), \\ z(t) = Ce(t), \\ y(t) = Ce(t) + \psi_d. \end{cases} \tag{5}$$

For nonlinear system (5), it is not easy to design a controller for the system directly. As is well-known, Takagi–Sugeno (T-S) model is commonly used to describe nonlinear systems. Therefore, system model (5) can be modeled as system model (6) via the nonlinear fuzzy aggregation of local linear input–output models.

$$\boldsymbol{R_i}: \text{IF } x_1(t) \text{ is } M_{i1} \text{ and } \dots \text{ and } x_n(t) \text{ is } M_{in},$$
$$\text{THEN} \begin{cases} \dot{e}(t) = A_i e(t) + B_i u(t) + D_i\varpi(t) \\ z(t) = C_i e(t) \\ y(t) = C_i e(t) + \psi_d \end{cases}, (i = 1, 2, \dots, r), \tag{6}$$

where $\boldsymbol{R_i}$ denotes the ith rule; r is the number of rules; $x_1(t), x_2(t), \dots, x_n(t)$ is premise variable; $M_{ij}(j = 1, 2, \dots, n)$ is fuzzy set; $A_i \in \mathbb{R}^{2\times2}$, $B_i \in \mathbb{R}^{2\times1}$, $C_i \in \mathbb{R}^{1\times2}$, $D_i \in \mathbb{R}^{2\times2}$ are real constant matrices.

Remark 2. It should be noted that (A_i, B_i) is controllable and (A_i, C_i) is observable.

Then, the system model (6) is fuzzified, and the global fuzzy system model corresponding to the system model (7) can be obtained, represented as follows

$$\begin{cases} \dot{e}(t) = \sum_{i=1}^{r} h_i(x(t))[A_i e(t) + B_i u(t) + D_i\varpi(t)], \\ z(t) = \sum_{i=1}^{r} h_i(x(t))[C_i e(t)], \\ y(t) = \sum_{i=1}^{r} h_i(x(t))[C_i e(t) + \psi_d], \end{cases} \tag{7}$$

where

$$x(t) = [x_1(t), x_2(t), \dots, x_n(t)],$$

$$h_i(x(t)) = w_i(x(t)) / \sum_{i=1}^{r} w_i(x(t)),$$

$$w_i(x(t)) = \prod_{j=1}^{n} M_{ij}(x_j(t)).$$

As per the fuzzy sets theory, we know that the following two inequalities are satisfied

$$\begin{matrix} w_i(x(t)) \ge 0, \sum_{i=1}^{r} w_i(x(t)) > 0, i = 1, 2, \dots, r, \\ h_i(x(t)) \ge 0, \sum_{i=1}^{r} h_i(x(t)) = 1, i = 1, 2, \dots, r. \end{matrix} \tag{8}$$

Having completed the fuzzy modeling of NSA system (system model (7)), the following experiments are conducted to verify the feasibility of system model (7). Firstly, the control rudder angle δ (actual control input u_a) and the actual heading angle ψ(actual output y_a) of "Qingshan" ship in course tracking situations were collected. Subsequently, u_a is taken as the control input of system model (7), i.e., $u = u_a$, and the estimated output y_o of system model (7) can be obtained. Further, with the comparison analysis of y_a and y_o, we can conclude that system model (7) is feasible. The framework and results of model feasibility analysis are presented in Figs. 2 and 3, respectively.

From Fig. 3, it is not difficult to see that the deviation ε between the actual output y_a and the estimated output y_o are observed when system model (7) is used to describe the actual NSA system. However, such deviations are natural and understandable. The reasons for this deviation are discussed in Remark 3. Consequently, we conclude that the system model (7) is feasible and it is capable of approximating the actual NSA system.

Remark 3. As stated in [28,29], the process of modeling is an abstraction and simplification of the system structural parameters. It is known that the mathematical model can only approximate the description of an actual system, and it is difficult to achieve a complete description of the actual system. Moreover, the controller used in the actual NSA system is different from the devised controller. Consequently, deviations between y_a and y_o are inevitable, especially when the ship receives a new command heading and makes adjustments. In summary, the system model (7) cannot match the actual NSA system completely, but can only approximate it, which leads to the fact that the deviation ε always exists. However, one can argue that system model (7) could be utilized to describe the actual NSA system as long as the deviations are natural and understandable.

Remark 4. In Fig. 4, the course tracking experiment was conducted with a scale model ("Qingshan" ship) in an inland river, and the actual navigation data of the scale model in course tracking situations were collected. It should be noted that these navigation data including the control rudder angle (actual control input u_a) and the actual heading angle (actual output y_a) were collected from 14:44:51 to 14:50:04. The parameters setting for course tracking experiment are given in Table 1. According to the real-time meteorological information, the water wave height h < 0.1 m and the wind level w < 0.1 during the period from 14:44:51 to 14:50:04. Combined with the actual navigation environment given in Fig. 4, one can see that the wind and wave disturbances on the water surface were relatively small at that time.

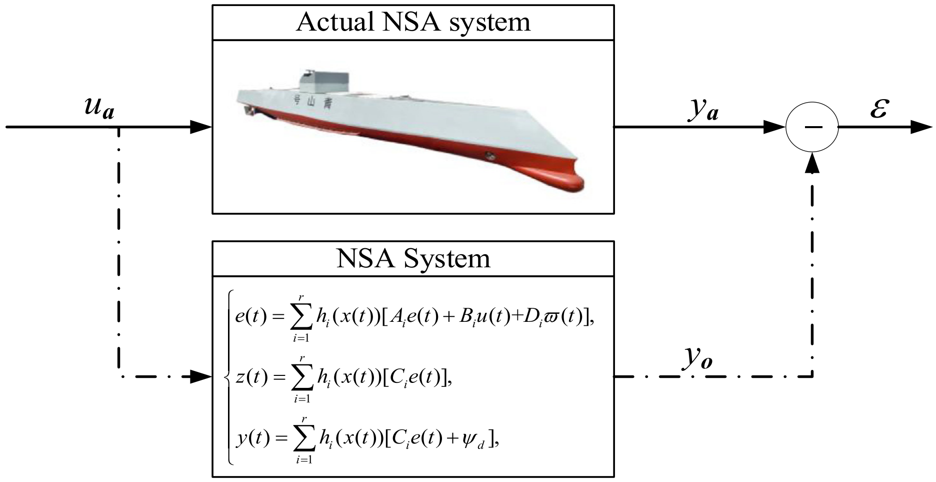

Fig. 2. Framework for model feasibility analysis.

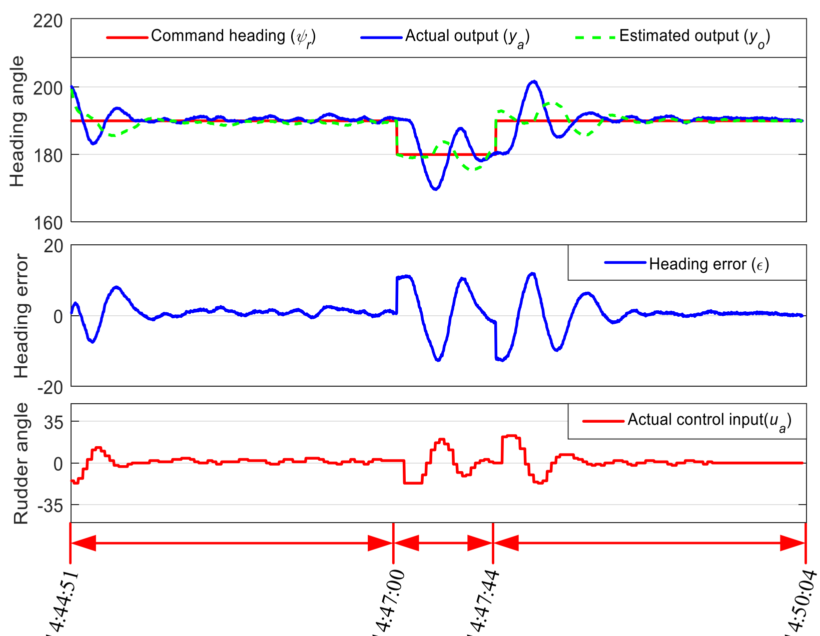

Fig. 3. Results (actual and estimated output) of model feasibility analysis.

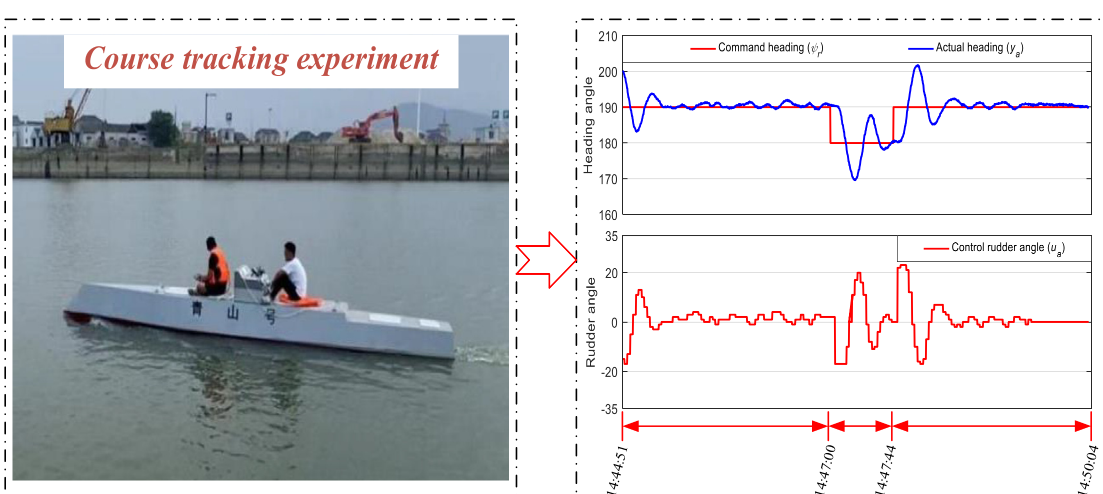

Fig. 4. Actual navigation data collected in course tracking situations.

Table 1
The parametesr setting for course tracking experiment.

Time	Command heading ψ_r
$t \in [14:44:51, 14:47:00)$	190°
$t \in [14:47:00, 14:47:44)$	180°
$t \in [14:47:44, 14:50:04]$	190°

2.2. Preliminaries

In this paper, we investigate a common steering machine bias fault. Specifically, both the fault-free (no steering machine bias fault) and faulty (bias fault) situations are considered. When there is no bias fault, the control input $u(t)$ is normal. While the bias fault occurs, the control input $u(t)$ is rewritten as

$$u(t) = u_f(t) + \bar{d}_a(t), \tag{9}$$

where $u_f(t)$ is control input signal and $\bar{d}_a(t)$ denotes the unknown bias fault.

The following assumptions, definitions, and theorems are needed to yield the main results.

Remark 5. The steering machine is an actuating component that manipulates the rotation of the ship's rudder blade in autopilot. In the automatic control system, the steering machine refers to the actuator. Typically, actuator faults include partial, outage, and bias modes. In this paper, we concentrate on the actuator bias fault with an irreversible state. In existing studies, the steering machine bias fault is usually modeled as an unknown additive function [30–32]. Consequently, it is feasible to adopt the fault model (9).

Assumption 1. The external disturbances ω is time-varying yet bounded, which means that the external disturbance satisfies $\omega(t) \in \mathfrak{L}_2[0,\infty)$.

Assumption 2. The desired heading ψ_d is a smooth signal with bounded derivatives $\dot{\psi}_d$ and $\ddot{\psi}_d$ which satisfy $\dot{\psi}_d \in \mathfrak{L}_2[0,\infty)$ and $\ddot{\psi}_d \in \mathfrak{L}_2[0,\infty)$.

Assumption 3. $\dot{\bar{d}}_a(t) \in \mathfrak{L}_2[0,\infty)$ is satisfied.

Remark 6. Defining the command heading as ψ_r, then ψ_d can be yielded according to the model reference technique [33]. The reference model is expressed as

$$\psi_d = \frac{\omega_n^2}{s^2 + 2\xi\omega_n s + \omega_n^2}\psi_r \tag{10}$$

where ξ and ω_n respectively denote the damping ratio and natural frequency of the reference model. It is worth noting that the selection of ξ and ω_n needs to be compatible with the ship steering performance so that the closed-loop system can perform better tracking speed and stability, which is usually taken as $0.8 \le \xi \le 1.0$.

Remark 7. As stated by Du et al. [11], the reference model (10) can be interpreted as a pre-filter for the commanded heading angle. It is sufficient to generate the smoothed desired heading ψ_d that satisfies Assumption 2 by using reference model (10). Such smoothed desired heading is more consistent with the course changing of ships in actual navigation.

Remark 8. Assumption 3 indicates that the fault derivative is energy-bounded. As described by Zhang et al. [34] and Huang and Yang [35], it is feasible to consider a fault that satisfies such an assumption in practice.

Definition 1 ([36,37]). A system is said to have H_∞ performance if a scalar $\gamma > 0$ exists that enables the following inequality holds under the zero initial condition:

$$\mathbb{E}\left\{\int_0^t x^{\mathrm{T}}(s)x(s)ds\right\} \le \gamma^2\mathbb{E}\left\{\int_0^t \omega^{\mathrm{T}}(s)\omega(s)ds\right\}, \forall t > 0,$$

where $x(s)$ is the system state vector.

Lemma 1 ([38,39]). *For a given symmetric matrix*

$$\mathcal{R} = \begin{bmatrix} \mathcal{R}_{11} & \mathcal{R}_{12} \\ \mathcal{R}_{12}^{\mathrm{T}} & \mathcal{R}_{22} \end{bmatrix},$$

where $\mathcal{R}_{11} \in \mathbb{R}^{n\times n}$, then the inequalities (1)–(3) are equivalent:

1. $\mathcal{R} < 0$;
2. $\mathcal{R}_{11} < 0, \mathcal{R}_{22} - \mathcal{R}_{12}^{\mathrm{T}}\mathcal{R}_{11}^{-1}\mathcal{R}_{12} < 0$;
3. $\mathcal{R}_{22} < 0, \mathcal{R}_{11} - \mathcal{R}_{12}\mathcal{R}_{22}^{-1}\mathcal{R}_{12}^{\mathrm{T}} < 0$.

3. Observer-based H_∞ fuzzy fault-tolerant switching control for ship course tracking control

To facilitate the NSA to meet different navigation conditions and scenarios and further improve the stability of course tracking control, the following switching control scheme for NSA system is proposed. Confronted with the challenge that system states are not easily measured or cannot be measured directly in practical engineering, Section 3.1 first designs VFOs for fault-free (observer 1) and faulty (observer 2) systems separately to estimate both the unmeasured states and unknown steering machine fault. This reduces the sensor cost and improves the applicability of controller for NSA systems equipped with low-cost sensors as well. To reduce the conservativeness of the NSA system caused by using a fault-tolerant controller even in fault-free situations, based on the VFOs, Section 3.2 designs the VFO-HRC (controller 1) and VFO-HFTC (controller 2) for fault-free and faulty systems, respectively. For accurate and effective fault detection and alarm, Section 3.3 develops the Z-score-based FDA to detect fault promptly and efficiently, and the switching signal (S_W) is generated to invoke the appropriate controller and corresponding observer. The switching control scheme with integrated VFOs, VFO-HRC, VFO-HFTC, and FDA for NSA system is described in Fig. 5.

3.1. VFO design

In this paper, two cases, fault-free (no steering machine fault) and faulty (bias fault) situations, are considered. Firstly, according to the definition of Lyapunov stability, Theorem 1 is given to obtain the observer gain L_{i1} without perturbations in fault-free situations. Subsequently, the observer L_{i2} is designed for the NSA system with faults, and the observer stability condition is given in Theorem 2.

Case 1: In fault-free situations, the global fuzzy system is given

$$\begin{cases} \dot{e}(t) = \sum_{i=1}^{r} h_i(x(t))[A_ie(t) + B_iu(t) + D_i\varpi(t)], \\ z(t) = \sum_{i=1}^{r} h_i(x(t))[C_ie(t)], \\ y(t) = \sum_{i=1}^{r} h_i(x(t))[C_ie(t) + \psi_d]. \end{cases} \tag{11}$$

In this case, the following VFO is designed for system (11).

$$\begin{cases} \dot{\theta}(t) = \sum_{i=1}^{r} h_i(x(t))\left[\mathcal{A}_i\theta(t) + \mathcal{B}_iu(t) + \mathcal{L}_iz(t)\right], \\ \hat{e}(t) = \theta(t), \\ \hat{y}(t) = \mathcal{C}_i\theta(t) + \psi_d, \end{cases} \tag{12}$$

where the VFO parameters can be described as $\theta(t)$, auxiliary state variable; $\mathcal{A}_i, \mathcal{B}_i, \mathcal{C}_i$, virtual system matrix; $\mathcal{L}_i$, virtual observer gain.

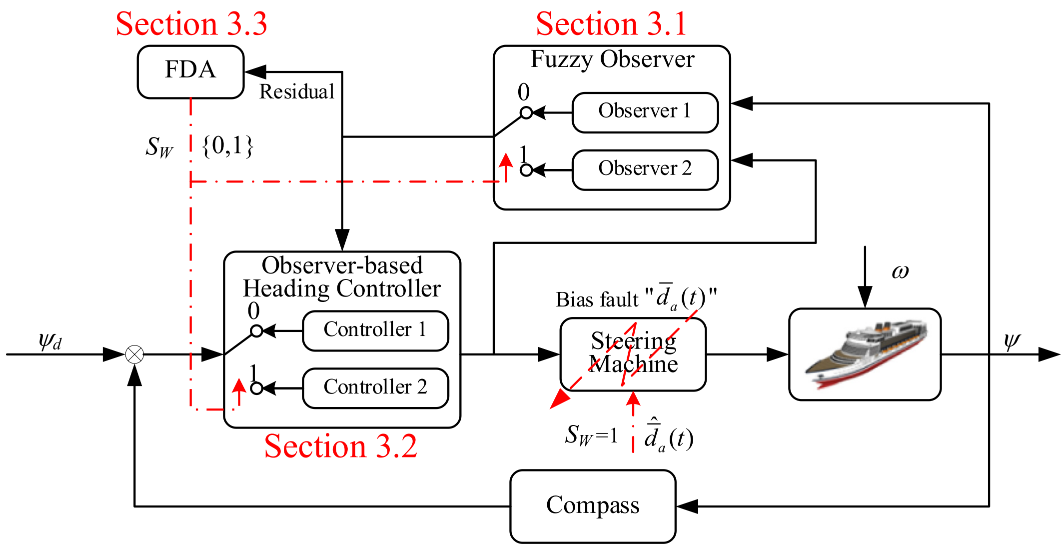

Fig. 5. Block diagram of the switching control scheme for NSA system.

For system (11), the following T-S fuzzy observer can be designed

$$\dot{\hat{e}}(t)=\sum_{i=1}^{r}h_i(x(t))[A_i\hat{e}(t)+B_iu(t)+L_{i1}(y(t)-\hat{y}(t))] \tag{13}$$

where $\hat{e}(t)$, $\hat{z}(t) = \sum_{i=1}^{r}h_i(x(t))[C_i\hat{e}(t)]$ and $\hat{y}(t) = \sum_{i=1}^{r}h_i(x(t))[C_i\hat{e}(t)+\psi_d]$ denote the state, tuned output, and control output of the observer, respectively, and L_{i1} is the observer gain to be designed.

Next, the state error $e_E(t)=e(t)-\hat{e}(t)$ of the system is defined, and the observation error dynamical system in Eq. (14) can be obtained from Eqs. (11) and (13).

$$\dot{e}_E(t)=\sum_{i=1}^{r}h_i(x(t))\,[(A_i-L_{i1}C_i)e_E(t)+D_i\varpi(t)] \tag{14}$$

Theorem 1. *For system (14), if there exist symmetric matrix $P>0$ and scalar $\gamma>0$, satisfying the following inequality*

$$\Xi_{o1}=\begin{bmatrix}\Theta_{11}' & \Theta_{12}\\ * & -\gamma^2 I\end{bmatrix}<0, \tag{15}$$

where

$$\Theta_{11}'=A_i^{\mathrm{T}}P+PA_i-Y_{o1}C_i-C_i^{\mathrm{T}}Y_{o1}^{\mathrm{T}}+I,$$

then the asymptotic stability of system (14) with H_∞ performance γ is guaranteed by observer (12), and the corresponding observer gain matrix L_{i1} can be obtained by $L_{i1}=P^{-1}Y_{o1}$. And the parameters of T-S fuzzy observer (12) are designed as follows.

$$\mathcal{A}_i=A_i-L_{i1}C_i,\ \mathcal{B}_i=B_i,\ \mathcal{C}_i=C_i,\ \mathcal{L}_i=L_{i1}. \tag{16}$$

Proof. : For system (14), the following Lyapunov-Krasovskii functional can be constructed:

$$V(t)=e_E^{\mathrm{T}}(t)Pe_E(t), \tag{17}$$

where $P>0$. Then, combining system (14), we obtain

$$\begin{aligned}\dot{V}(t)&=2\dot{e}_E^{\mathrm{T}}(t)Pe_E(t)\\ &=\sum_{i=1}^{r}h_i(x(t))\begin{bmatrix}(A_ie_E(t)-L_{i1}C_ie_E(t)+D_i\varpi(t))^{\mathrm{T}}Pe_E(t)\\ +e_E^{\mathrm{T}}(t)P(A_ie_E(t)-L_{i1}C_ie_E(t)+D_i\varpi(t))\end{bmatrix},\end{aligned}$$

Subsequently, let

$$H(t)=\dot{V}(t)+e_E^{\mathrm{T}}(t)e_E(t)-\gamma^2\varpi^{\mathrm{T}}(t)\varpi(t), \tag{18}$$

then we can obtain that

$$H(t)\le\eta(t)\Xi_o\eta^{\mathrm{T}}(t),$$

where

$$\eta(t)=[e_E^{\mathrm{T}}(t)\varpi^{\mathrm{T}}(t)],\ \ \Xi_o=\begin{bmatrix}\Theta_{11}+I & \Theta_{12}\\ * & -\gamma^2 I\end{bmatrix},$$

$$\Theta_{11}=(A_i-L_{i1}C_i)^{\mathrm{T}}P+P(A_i-L_{i1}C_i),\ \ \Theta_{12}=PD_i.$$

Further, noting $Y_{o1}=PL_{i1}$ and substituting it into Ξ_o, then Ξ_{o1} is easily obtained.

When $\varpi(t)=0$, LMI (15) guarantees $\dot{V}(t)<0$, which means that the observation error dynamical system (14) is asymptotically stable. When $\varpi(t)=0$, simultaneously integrating both sides of (18) yields

$$\begin{aligned}&\mathbb{E}\left\{\int_0^t[e_E^T(s)e_E(s)-\gamma^2\varpi^T(s)\varpi(s)]ds\right\}\\ &=\mathbb{E}\left\{\int_0^t[H(s)-\dot{V}(s)]ds\right\}\le-\mathbb{E}\left\{\int_0^t\dot{V}(s)ds\right\}\\ &=\mathbb{E}\{V(0)\}-\mathbb{E}\{V(t)\}\le 0.\end{aligned} \tag{19}$$

As a result, the system (14) is easily proved to have H_∞ performance γ according to Definition 1. That is, the system (14) is asymptotically stable with disturbance attenuation level γ when LMI (15) holds.

Let $\theta(t)=\hat{e}(t)$, then the T-S fuzzy observer (13) can be rewritten as

$$\begin{aligned}\dot{\theta}(t)&=\sum_{i=1}^{r}h_i(x(t))\left[A_i\theta(t)+B_iu(t)+L_{i1}(y(t)-\hat{y}(t))\right]\\ &=\sum_{i=1}^{r}h_i(x(t))\left[A_i\theta(t)+B_iu(t)+L_{i1}(z(t)-\hat{z}(t))\right]\\ &=\sum_{i=1}^{r}h_i(x(t))\left[(A_i-L_{i1}C_i)\theta(t)+B_iu(t)+L_{i1}z(t)\right].\end{aligned}$$

Accordingly, it also yields $\hat{e}(t)=\theta(t)$. Simultaneously, one can obtain the design parameters of observer (12).

Case 2: In faulty situations, the global fuzzy system is given

$$\left\{\begin{aligned}\dot{e}(t)&=\sum_{i=1}^{r}h_i(x(t))[A_ie(t)+B_i(u_f(t)+\bar{d}_a(t))+D_i\varpi(t)],\\ z(t)&=\sum_{i=1}^{r}h_i(x(t))[C_ie(t)],\\ y(t)&=\sum_{i=1}^{r}h_i(x(t))[C_ie(t)+\psi_d].\end{aligned}\right. \tag{20}$$

In this case, the following VFO is designed for system (20).

$$\left\{\begin{aligned}\dot{\bar{\theta}}(t)&=\sum_{i=1}^{r}h_i(x(t))\left[\bar{\mathcal{A}}_i\bar{\theta}(t)+\bar{\mathcal{B}}_iu_f(t)+\bar{\mathcal{L}}_iz(t)\right],\\ \hat{\bar{e}}(t)&=\bar{\theta}(t)+\bar{\mathcal{C}}_iz(t),\\ \hat{y}(t)&=\bar{\mathcal{G}}_2\bar{\theta}(t)+\bar{\mathcal{G}}_2\bar{\mathcal{C}}_iz(t)+\psi_d,\end{aligned}\right. \tag{21}$$

where the VFO parameters can be described as $\overline{\theta}(t)$, auxiliary state variable; $\overline{\mathcal{A}}_i, \overline{\mathcal{B}}_i, \overline{\mathcal{C}}_i$, virtual system matrix; $\overline{\mathcal{L}}_i$, virtual observer gain.

For system (20), letting $\overline{e}(t) = [e^{\mathrm{T}}(t)\overline{d}_a^{\mathrm{T}}(t)]^{\mathrm{T}}$, then we can obtain its augmented system, denoted as

$$\begin{cases} \overline{\mathcal{G}}_1\dot{\overline{e}}(t) = \sum_{i=1}^r h_i(x(t))[A_{i2}\overline{e}(t) + B_i u_f(t) + D_i\varpi(t)], \\ z(t) = \sum_{i=1}^r h_i(x(t))[\overline{\mathcal{G}}_2\overline{e}(t)], \\ y(t) = \sum_{i=1}^r h_i(x(t))[\overline{\mathcal{G}}_2\overline{e}(t) + \psi_d]. \end{cases} \tag{22}$$

where $A_{i2} = [A_i\ B_i], \overline{\mathcal{G}}_1 = [I_2\ 0_{2\times 1}], \overline{\mathcal{G}}_2 = [C_i\ 0]$;

Defining $\overline{\mathcal{G}}_3 = [C_i \quad I]$, then $rank([\overline{\mathcal{G}}_1^{\mathrm{T}} \quad \overline{\mathcal{G}}_3^{\mathrm{T}}]^{\mathrm{T}}) = rank\left(\begin{bmatrix} I_2 & 0_{2\times 1} \\ C_i & I \end{bmatrix}\right) = 3$, which means that the inverse of $[\overline{\mathcal{G}}_1^{\mathrm{T}}\ \overline{\mathcal{G}}_3^{\mathrm{T}}]^{\mathrm{T}}$ exists.

Subsequently, letting $\overline{\mathcal{Q}}_1 = [I_2^{\mathrm{T}} - C_i^{\mathrm{T}}]^{\mathrm{T}}$ and $\overline{\mathcal{Q}}_2 = [0_{2\times 1}^{\mathrm{T}} I^{\mathrm{T}}]^{\mathrm{T}}$, then we can obtain

$$[\overline{\mathcal{Q}}_1\ \overline{\mathcal{Q}}_2][\overline{\mathcal{G}}_1^{\mathrm{T}}\ \overline{\mathcal{G}}_3^{\mathrm{T}}]^{\mathrm{T}} = [\overline{\mathcal{G}}_1^{\mathrm{T}}\ \overline{\mathcal{G}}_3^{\mathrm{T}}]^{\mathrm{T}}[\overline{\mathcal{Q}}_1\ \overline{\mathcal{Q}}_2] = I_3. \tag{23}$$

From (23), we know that $[\overline{\mathcal{G}}_1^{\mathrm{T}}\ \overline{\mathcal{G}}_3^{\mathrm{T}}]^{-\mathrm{T}} = [\overline{\mathcal{Q}}_1\ \overline{\mathcal{Q}}_2]$.

Next, multiplying $\overline{\mathcal{Q}}_1$ to both sides of system (22) and adding $\overline{\mathcal{Q}}_2\overline{\mathcal{G}}_3\dot{\overline{e}}(t)$ yields

$$\dot{\overline{e}}(t) = \sum_{i=1}^r h_i(x(t))[\overline{\mathcal{Q}}_1A_{i2}\overline{e}(t) + \overline{\mathcal{Q}}_1B_iu_f(t) + \overline{\mathcal{Q}}_1D_i\varpi(t) + \overline{\mathcal{Q}}_2\overline{\mathcal{G}}_3\dot{\overline{e}}(t)]. \tag{24}$$

Then, the following T-S fuzzy observer can be designed

$$\begin{aligned}\dot{\widehat{\overline{e}}}(t) = \sum_{i=1}^r h_i(x(t))[&\overline{\mathcal{Q}}_1A_{i2}\widehat{\overline{e}}(t) + \overline{\mathcal{Q}}_1B_iu_f(t) + \overline{\mathcal{Q}}_2\overline{\mathcal{G}}_2\dot{\overline{e}}(t) \\ &+ L_{i2}(y(t) - \hat{y}(t))],\end{aligned} \tag{25}$$

where $\widehat{\overline{e}}(t)$, $\hat{z}(t) = \sum_{i=1}^r h_i(x(t))[\overline{\mathcal{G}}_2\widehat{\overline{e}}(t)]$ and $\hat{y}(t) = \sum_{i=1}^r h_i(x(t))[\overline{\mathcal{G}}_2\widehat{\overline{e}}(t) + \psi_d]$ denote the state, tuned output, and control output of the observer, respectively, and L_{i2} is the observer gain to be designed.

Subsequently, the state error $\overline{e}_E(t) = \overline{e}(t) - \widehat{\overline{e}}(t)$ of the system is defined, and the observation error dynamical system in Eq. (26) can be obtained from Eqs. (24) and (25).

$$\dot{\overline{e}}_E(t) = \sum_{i=1}^r h_i(x(t))[(\overline{\mathcal{Q}}_1A_{i2} - L_{i2}\overline{\mathcal{G}}_2)\overline{e}_E(t) + \overline{\mathcal{Q}}_i\overline{\varpi}(t)], \tag{26}$$

where, $\overline{\mathcal{Q}}_i = [\overline{\mathcal{Q}}_1D_i\overline{\mathcal{Q}}_2]$, $\overline{\varpi}(t) = [\varpi^{\mathrm{T}}(t)\dot{\overline{d}}_a^{\mathrm{T}}(t)]^{\mathrm{T}}$.

Theorem 2. *For system (26), if there exist symmetric matrix $P > 0$, scalar $\gamma > 0$, and any invertible matrix N with appropriate dimensions, satisfying the following inequality*

$$\Xi_{o2} = \begin{bmatrix} \overline{\Theta}'_{11} + I & \overline{\Theta}'_{12} & \overline{\Theta}_{13} \\ * & \overline{\Theta}_{22} & \overline{\Theta}_{23} \\ * & * & -\overline{\gamma}^2 I \end{bmatrix} < 0, \tag{27}$$

where

$$\overline{\Theta}'_{11} = \sigma_1N\overline{\mathcal{Q}}_1A_{i2} - \sigma_1Y_{o2}\overline{\mathcal{G}}_2 + \sigma_1A_{i2}^{\mathrm{T}}\overline{\mathcal{Q}}_1^{\mathrm{T}}N^{\mathrm{T}} - \sigma_1\overline{\mathcal{G}}_2^{\mathrm{T}}Y_{o2}^{\mathrm{T}},$$

$$\overline{\Theta}'_{12} = -\sigma_1N + \sigma_2A_{i2}^{\mathrm{T}}\overline{\mathcal{Q}}_1^{\mathrm{T}}N^{\mathrm{T}} - \sigma_2\overline{\mathcal{G}}_2^{\mathrm{T}}Y_{o2}^{\mathrm{T}} + P,$$

then the asymptotic stability of system (26) with H_∞ performance $\overline{\gamma}$ is guaranteed by observer (21), and the corresponding observer gain matrix L_{i2} can be obtained by $L_{i2} = N^{-1}Y_{o2}$. And the parameters of T-S fuzzy observer (21) are designed as follows.

$$\overline{\mathcal{A}}_i = \overline{\mathcal{Q}}_1A_{i2} - L_{i2}\overline{\mathcal{G}}_2, \overline{\mathcal{B}}_i = \overline{\mathcal{Q}}_1B_i, \overline{\mathcal{C}}_i = \overline{\mathcal{Q}}_2S,$$
$$\overline{\mathcal{L}}_i = L_{i2} + (\overline{\mathcal{Q}}_1A_{i2} - L_{i2}\overline{\mathcal{G}}_2)\overline{\mathcal{Q}}_2 \tag{28}$$

Proof (:). For system (26), the following Lyapunov-Krasovskii functional can be constructed:

$$V_a(t) = \overline{e}_E^{\mathrm{T}}(t)P\overline{e}_E(t), \tag{29}$$

where $P > 0$. Next, combining system (26), we obtain

$$\dot{V}_a(t) = \dot{\overline{e}}_E^{\mathrm{T}}(t)P\overline{e}_E(t) + \overline{e}_E^{\mathrm{T}}(t)P\dot{\overline{e}}_E(t).$$

For some given scalars $\sigma_1 > 0$, $\sigma_2 > 0$, and any invertible matrix N with appropriate dimensions, we can obtain that

$$\begin{aligned} 0 = 2&\left[-\overline{e}_E^{\mathrm{T}}(t)\sigma_1N - \dot{\overline{e}}_E^{\mathrm{T}}(t)\sigma_2N\right] \\ \times&\left[\dot{\overline{e}}_E(t) - (\overline{\mathcal{Q}}_1A_{i2} - L_{i2}\overline{\mathcal{G}}_2)\overline{e}_E(t) - \overline{\mathcal{Q}}_i\overline{\varpi}(t)\right].\end{aligned}$$

Further, let

$$H(t) = \dot{V}_a(t) + \overline{e}_E^{\mathrm{T}}(t)\overline{e}_E(t) - \overline{\gamma}^2\overline{\varpi}^{\mathrm{T}}(t)\overline{\varpi},(t)\,\eta(t) = [\overline{e}_E^{\mathrm{T}}(t)\dot{\overline{e}}_E^{\mathrm{T}}(t)\overline{\varpi}^{\mathrm{T}}(t)],$$

then we can induce that

$$H(t) \leq \eta(t)\Xi_o\eta^T(t),$$

where

$$\Xi_o = \begin{bmatrix} \overline{\Theta}_{11} + I & \overline{\Theta}_{12} & \overline{\Theta}_{13} \\ * & \overline{\Theta}_{22} & \overline{\Theta}_{23} \\ * & * & -\overline{\gamma}^2 I \end{bmatrix},$$

$$\overline{\Theta}_{11} = \sigma_1N\overline{\mathcal{Q}}_1A_{i2} - \sigma_1NL_{i2}\overline{\mathcal{G}}_2 + \sigma_1A_{i2}^{\mathrm{T}}\overline{\mathcal{Q}}_1^{\mathrm{T}}N^{\mathrm{T}} - \sigma_1\overline{\mathcal{G}}_2^{\mathrm{T}}L_{i2}^{\mathrm{T}}N^{\mathrm{T}},$$

$$\overline{\Theta}_{12} = -\sigma_1N + \sigma_2A_{i2}^{\mathrm{T}}\overline{\mathcal{Q}}_1^{\mathrm{T}}N^{\mathrm{T}} - \sigma_2\overline{\mathcal{G}}_2^{\mathrm{T}}L_{i2}^{\mathrm{T}}N^{\mathrm{T}} + P,$$

$$\overline{\Theta}_{13} = \sigma_1N\overline{\mathcal{Q}}_i, \overline{\Theta}_{22} = -\sigma_2N - \sigma_2N^{\mathrm{T}}, \overline{\Theta}_{23} = \sigma_2N\overline{\mathcal{Q}}_i.$$

Subsequently, noting $Y_{o2} = NL_{i2}$ and substituting it into Ξ_o, then Ξ_{o2} is easily obtained.

Similar to Theorem 1, the system (26) is easily proved to be asymptotically stable with disturbance attenuation level $\overline{\gamma}$ when LMI (27) holds. And when $\varpi(t) \neq 0$, we have

$$\begin{aligned} &\mathbb{E}\left\{\int_0^t[\overline{e}_E^T(s)\overline{e}_E(s) - \overline{\gamma}^2\overline{\varpi}^T(s)\overline{\varpi}(s)]ds\right\} = \mathbb{E}\left\{\int_0^t[H(s) - \dot{V}_a(s)]ds\right\} \\ &\leq -\mathbb{E}\left\{\int_0^t \dot{V}_a(s)ds\right\} \\ &= \mathbb{E}\{V_a(0)\} - \mathbb{E}\{V_a(t)\} \leq 0. \end{aligned} \tag{30}$$

To remove $\overline{\mathcal{Q}}_2\overline{\mathcal{G}}_2\dot{\overline{e}}(t)$ from the T-S fuzzy observer (25), $\overline{\theta}(t) = \widehat{\overline{e}}(t) - \overline{\mathcal{Q}}_2\overline{\mathcal{G}}_2\overline{e}(t)$ is further defined, then the system (25) can be rewritten as

$$\begin{aligned}\dot{\overline{\theta}}(t) &= \textstyle\sum_{i=1}^r h_i(x(t))\left[\overline{\mathcal{Q}}_1A_{i2}\widehat{\overline{e}}(t) + \overline{\mathcal{Q}}_1B_iu_f(t) + L_{i2}(y(t) - \hat{y}(t))\right] \\ &= \textstyle\sum_{i=1}^r h_i(x(t))\left[\overline{\mathcal{Q}}_1A_{i2}\widehat{\overline{e}}(t) + \overline{\mathcal{Q}}_1B_iu_f(t) + L_{i2}(z(t) - \hat{z}(t))\right] \\ &= \textstyle\sum_{i=1}^r h_i(x(t))\begin{bmatrix} (\overline{\mathcal{Q}}_1A_{i2} - L_{i2}\overline{\mathcal{G}}_2)\overline{\theta}(t) + \overline{\mathcal{Q}}_1B_iu_f(t) \\ +(L_{i2} + (\overline{\mathcal{Q}}_1A_{i2} - L_{i2}\overline{\mathcal{G}}_2)\overline{\mathcal{Q}}_2)z(t)\end{bmatrix}.\end{aligned}$$

Accordingly, it also yields $\widehat{\overline{e}}(t) = \overline{\theta}(t) + \overline{\mathcal{Q}}_2\overline{\mathcal{G}}_2\overline{e}(t) = \overline{\theta}(t) + \overline{\mathcal{Q}}_2z(t)$. Then, one can obtain the design parameters of observer (21).

3.2. VFO-based HRC and HFTC design

Based on the VFOs designed in Section 3.1, VFO-based HRC and HFTC are designed in Section 3.2. Specifically, based on the VFOs designed in Case 1 of Section 3.1, VFO-HRC is designed in Case 3 and the stability condition of VFO-HRC is given in Theorem 3. Meanwhile, based on the VFO designed in Case 2 of Section 3.1, the VFO-HFTC is designed in Case 4 and the stability condition of VFO-HFTC is given in Theorem 4.

Case 3: To stabilize system (11), the following global fuzzy robust controllers need to be considered.

$$u(t)=\sum_{i=1}^{r}h_i(x(t))[K_{i1}\hat{e}(t)], \tag{31}$$

where $K_{i2}\in\mathbb{R}^{1\times 2}$ is the controller gain matrix.

Substituting (31) into (11), then we have

$$\begin{aligned}\dot{e}(t)&=\sum_{i=1}^{r}\sum_{j=1}^{r}h_i(x(t))h_j(x(t))[A_ie(t)+B_iK_{i1}\hat{e}(t)+D_i\varpi(t)]\\&=\sum_{i=1}^{r}\sum_{j=1}^{r}h_i(x(t))h_j(x(t))[(A_i+B_iK_{i1})e(t)-B_iK_{i1}e_E(t)+D_i\varpi(t)]\\&=\sum_{i=1}^{r}\sum_{j=1}^{r}h_i(x(t))h_j(x(t))[(A_i+B_iK_{i1})e(t)-B_iv_{i1}(t)+D_i\varpi(t)],\end{aligned} \tag{32}$$

where $\overline{v}_{i1}(t)=K_{i1}e_E(t)$.

Theorem 3. *For observer (12), if there exist scalars $\gamma'>0$, $\alpha_1>0$, symmetric matrix $\overline{P}>0$, and any invertible matrix $\widehat{\overline{P}}$ with appropriate dimensions, satisfying the following inequality*

$$\varXi_{c1}=\begin{bmatrix}\overleftrightarrow{\varTheta}'_{11} & \widehat{\overline{P}} & -B_i & D_i\\ * & -I & 0 & 0\\ * & * & -\alpha_1 I & 0\\ * & * & * & -\gamma^2 I\end{bmatrix}<0, \tag{33}$$

where

$$\overleftrightarrow{\varTheta}'_{11}=A_i\widehat{\overline{P}}+\widehat{\overline{P}}A_i^{\mathrm{T}}+B_iG+G^{\mathrm{T}}B_i^{\mathrm{T}},$$

$$\gamma'=(\alpha_1\lambda_{\max}(K_{i1}^TK_{i1})+1)^{1/2}\gamma,$$

then the asymptotic stability of system (32) with H_∞ performance γ' is guaranteed by controller (31), and the corresponding observer gain matrix K_{i1} can be obtained by $K_{i1}=G\widehat{\overline{P}}^{-1}$.

Proof (:)**.** For system (32), the following Lyapunov-Krasovskii functional can be constructed:

$$\overline{V}(t)=e^{\mathrm{T}}(t)\overline{P}e(t), \tag{34}$$

where $\overline{P}>0$. Then, combining system (32), we obtain

$$\dot{\overline{V}}(t)+e^{\mathrm{T}}(t)e(t)=\eta(t)\varXi_c\eta^T(t)+\alpha_1v_{i1}^{\mathrm{T}}(t)v_{i1}(t)+\gamma^2\varpi^{\mathrm{T}}(t)\varpi(t), \tag{35}$$

where

$$\eta(t)=[e^{\mathrm{T}}(t)v_{i1}^{\mathrm{T}}(t)\varpi^{\mathrm{T}}(t)],$$

$$\varXi_c=\begin{bmatrix}\overleftrightarrow{\varTheta}_{11} & -\overline{P}B_i & \overline{P}D_i\\ * & -\alpha_1 I & 0\\ * & * & -\gamma^2 I\end{bmatrix},$$

$$\widetilde{\varTheta}_{11}=\overline{P}A_i+A_i^{\mathrm{T}}\overline{P}+\overline{P}B_iK_{i1}+K_{i1}^{\mathrm{T}}B_i^{\mathrm{T}}\overline{P}+I.$$

Let $\widehat{\overline{P}}=\overline{P}^{-1}$ and multiply $diag\widehat{\overline{P}},I,I$ on the left and right of $\varXi_c$. Then, according to Lemma 1, $\varXi_{c1}$ can be obtained, which guarantees $\varXi_c<0$. Afterward, combining the system (19) and (35) yields

$$\dot{\overline{V}}(t)+e^{\mathrm{T}}(t)e(t)<\gamma^2\varpi^{\mathrm{T}}(t)\varpi(t)+\alpha_1v_{i1}^{\mathrm{T}}(t)v_{i1}(t).$$

Simultaneously integrating both sides of above equation yields

$$\begin{aligned}&\mathbb{E}\left\{\int_0^t e^T(s)e(s)ds\right\}\\&\le\mathbb{E}\left\{\int_0^t\left[\gamma^2\varpi^T(s)\varpi(s)+\alpha_1v_{i1}^T(s)v_{i1}(s)\right]ds\right\}\\&\le\mathbb{E}\left\{\int_0^t\left[\gamma^2\varpi^T(s)\varpi(s)+\alpha_1\lambda_{\max}(K_{i1}^TK_{i1})e_E^T(s)e_E(s)\right]ds\right\}\\&\le\mathbb{E}\left\{\int_0^t\left[\gamma^2\varpi^T(s)\varpi(s)+\alpha_1\lambda_{\max}(K_{i1}^TK_{i1})\gamma^2\varpi^T(s)\varpi(s)\right]ds\right\}\\&=\mathbb{E}\left\{\int_0^t\left[\gamma'^2\varpi^T(s)\varpi(s)\right]ds\right\},\end{aligned}$$

where γ' has been defined in Theorem 3. As a result, the system (32) is easily proved to have H_∞ performance γ' according to Definition 1. That is, the system (32) is asymptotically stable with disturbance attenuation level γ' when LMI (33) holds.

Case 4: To stabilize system (20), the following global fuzzy fault-tolerant controllers need to be considered.

$$u_f(t)=\sum_{i=1}^{r}h_i(x(t))[K_{i2}\hat{e}(t)-\widehat{\overline{d}}_a(t)]=\sum_{i=1}^{r}h_i(x(t))[(K_{i2}\overline{\mathcal{G}}_1-\overline{\mathcal{Q}}_2^{\mathrm{T}})\widehat{\overline{e}}(t)], \tag{36}$$

where $K_{i2}\in\mathcal{R}^{1\times 2}$ is the controller gain matrix.

Substituting (36) into (20), then we have

$$\begin{aligned}\dot{e}(t)&=\sum_{i=1}^{r}\sum_{j=1}^{r}h_i(x(t))h_j(x(t))\begin{bmatrix}A_ie(t)+B_i(K_{i2}\overline{\mathcal{G}}_1-\overline{\mathcal{Q}}_2^{\mathrm{T}})\widehat{\overline{e}}(t)\\+B_i\overline{d}_a(e(t),t)+D_i\varpi(t)\end{bmatrix}\\&=\sum_{i=1}^{r}\sum_{j=1}^{r}h_i(x(t))h_j(x(t))\begin{bmatrix}(A_i+B_iK_{i2})e(t)\\-B_i(K_{i2}\overline{\mathcal{G}}_1-\overline{\mathcal{Q}}_2^{\mathrm{T}})\overline{e}_E(t)+D_i\varpi(t)\end{bmatrix}\\&=\sum_{i=1}^{r}\sum_{j=1}^{r}h_i(x(t))h_j(x(t))\begin{bmatrix}(A_i+B_iK_{i2})e(t)-B_i\overline{v}_{i1}(t)\\+B_i\overline{v}_2(t)+\overline{D}_i\overline{\varpi}(t)\end{bmatrix},\end{aligned} \tag{37}$$

where $\overline{v}_{i1}(t)=K_{i2}\overline{\mathcal{G}}_1\overline{e}_E(t)$, $\overline{v}_2(t)=\overline{\mathcal{Q}}_2^{\mathrm{T}}\overline{e}_E(t)$, $\overline{D}_i=[D_i\,0]$.

Theorem 4. *For observer (21), if there exist scalars $\overline{\gamma}'>0$, $\overline{\alpha}_1>0$, $\overline{\alpha}_2>0$, symmetric matrix $\overline{P}>0$, and any invertible matrix $\widehat{\overline{P}}$ with appropriate dimensions, satisfying the following inequality*

$$\varXi_{c2}=\begin{bmatrix}\overleftrightarrow{\varTheta}'_{11} & \widehat{\overline{P}} & -B_i & B_i & \overline{D}_i\\ * & -I & 0 & 0 & 0\\ * & * & -\overline{\alpha}_1 I & 0 & 0\\ * & * & * & -\overline{\alpha}_2 I & 0\\ * & * & * & * & -\overline{\gamma}^2 I\end{bmatrix}<0, \tag{38}$$

where

$$\overleftrightarrow{\varTheta}'_{11}=A_i\widehat{\overline{P}}+\widehat{\overline{P}}A_i^{\mathrm{T}}+B_i\overline{G}+\overline{G}^{\mathrm{T}}B_i^{\mathrm{T}},$$

$$\overline{\gamma}'=(\overline{\alpha}_1\lambda_{\max}(K_{i2}^TK_{i2})+\overline{\alpha}_2+1)^{1/2}\overline{\gamma},$$

then the asymptotic stability of system (37) with H_∞ performance $\overline{\gamma}'$ is guaranteed by controller (36), and the corresponding observer gain matrix K_{i2} can be obtained by $K_{i2}=\overline{G}\widehat{\overline{P}}^{-1}$.

Proof (:)**.** For system (37), the following Lyapunov-Krasovskii functional can be constructed:

$$\overline{V}_a(t)=e^{\mathrm{T}}(t)\overline{P}e(t), \tag{39}$$

where $\overline{P}>0$. Next, combining system (37), we obtain

$$\begin{aligned}\dot{\overline{V}}_a(t)+e^{\mathrm{T}}(t)e(t)&=\eta(t)\overline{\varXi}_c\eta^T(t)+\overline{\alpha}_1\overline{v}_{i1}^{\mathrm{T}}(t)\overline{v}_{i1}(t)+\overline{\alpha}_2\overline{v}_2^{\mathrm{T}}(t)\overline{v}_2(t)\\&\quad+\overline{\gamma}^2\overline{\varpi}^{\mathrm{T}}(t)\overline{\varpi}(t)\end{aligned} \tag{40}$$

where

$\eta(t) = [e^{\mathrm{T}}(t)\overline{v}_{i1}^{\mathrm{T}}(t)\overline{v}_2^{\mathrm{T}}(t)\overline{\varpi}^{\mathrm{T}}(t)]$,

$$\overline{\Xi}_c = \begin{bmatrix} \overleftrightarrow{\overline{\Theta}}_{11} & -\overline{P}B_i & \overline{P}B_i & \overline{P}D_i \\ * & -\overline{\alpha}_1 I & 0 & 0 \\ * & * & -\overline{\alpha}_2 I & 0 \\ * & * & * & -\overline{\gamma}^2 I \end{bmatrix},$$

$\overleftrightarrow{\overline{\Theta}}_{11} = \overline{P}A_i + A_i^{\mathrm{T}}\overline{P} + \overline{P}B_i\overline{K}_{i2} + \overline{K}_{i2}^{\mathrm{T}}B_i^{\mathrm{T}}\overline{P} + I.$

Let $\widehat{\overline{P}} = \overline{P}^{-1}$ and multiply $diag\widehat{\overline{P}}, I, I, I$ on the left and right of $\overline{\Xi}$. Then, according to Lemma 1, Ξ_{c2} can be obtained, which guarantees $\overline{\Xi}_c < 0$. Afterwards, from (40), we can obtain

$$\dot{\overline{V}}_a(t) + e^{\mathrm{T}}(t)e(t) < \overline{\alpha}_1\overline{v}_{i1}^{\mathrm{T}}(t)\overline{v}_{i1}(t) + \overline{\alpha}_2\overline{v}_2^{\mathrm{T}}(t)\overline{v}_2(t) + \overline{\gamma}^2\overline{\varpi}^{\mathrm{T}}(t)\overline{\varpi}(t).$$

Simultaneously integrating both sides of above equation yields

$$\begin{aligned} &\mathbb{E}\left\{\int_0^t e^T(s)e(s)ds\right\} \\ &\leq \mathbb{E}\left\{\int_0^t \left[\overline{\alpha}_1\overline{v}_{i1}^T(s)\overline{v}_{i1}(s) + \overline{\alpha}_2\overline{v}_2^T(s)\overline{v}_2(s) + \overline{\gamma}^2\overline{\varpi}^T(s)\overline{\varpi}(s)\right]ds\right\} \\ &\leq \mathbb{E}\left\{\int_0^t \begin{bmatrix} \overline{\alpha}_1\lambda_{\max}(K_{i2}^TK_{i2})\overline{e}_E^T(s)\overline{\mathcal{G}}_1^T\overline{\mathcal{G}}_1\overline{e}_E(s) \\ +\overline{\alpha}_2\overline{e}_E^T(s)\overline{\mathcal{Q}}_2\overline{\mathcal{Q}}_2^T\overline{e}_E(s) + \overline{\gamma}^2\overline{\varpi}^T(s)\overline{\varpi}(s) \end{bmatrix} ds\right\} \\ &\leq \mathbb{E}\left\{\int_0^t \begin{bmatrix} \overline{\alpha}_1\lambda_{\max}(K_{i2}^TK_{i2})\overline{\gamma}^2\overline{\varpi}^T(s)\overline{\varpi}(s) \\ +\overline{\alpha}_2\overline{\gamma}^2\overline{\varpi}^T(s)\overline{\varpi}(s) + \overline{\gamma}^2\overline{\varpi}^T(s)\overline{\varpi}(s) \end{bmatrix} ds\right\} \\ &= \mathbb{E}\left\{\int_0^t \left[\overline{\gamma}'^2\overline{\varpi}^T(s)\overline{\varpi}(s)\right]ds\right\}, \end{aligned}$$

where $\overline{\gamma}'$ has been defined in Theorem 4. As a result, the system (37) is easily proved to have H_∞ performance $\overline{\gamma}'$ according to Definition 1. That is, the system (32) is asymptotically stable with disturbance attenuation level $\overline{\gamma}'$ when LMI (38) holds.

3.3. FDA design

For a smooth controlled healthy system, the residual is always zero. On the contrary, there must exist some fault when residual deviates from the origin of the system [40]. For that, an analysis of residual signal is carried out in this section, and a smoothed Z-score-based FDA is developed to efficiently detect steering machine fault and provide switching signals for invoking VFO-HFTC.

As we know, the continuous states can be assigned with discrete values. The reason for this is that states are usually continuous values with discrete sampling points. So, the continuous residual signal $x_e = |y - \hat{y}|$ can be sampled, and the mean $\bar{s}_k$ and standard deviation σ_{s_k} of the samples can be calculated as

$$\bar{s}_k = \frac{1}{l}\sum_{k}^{k+l} s_k, \tag{41-1}$$

$$\sigma_{s_k} = \sqrt{\frac{\sum_k^{k+l}(s_k - \bar{s}_k)^2}{l-1}}, \tag{41-2}$$

where l is the lag parameter, k denotes the kth sampling point $x_e(k)$, and s_k is the adjusted value of $x_e(k)$ after adding the influence parameter i_n $(0 \leq i_n \leq 1)$

$$s_k = i_n x_e(k) + (1 - i_n)s_{k-1}, \tag{42}$$

where i_n satisfies $0 \leq i_n \leq 1$.

Consequently, the Z-score corresponding to the kth sampling time (i.e., $t_k = kt_s$ and t_s is the sampling interval) can be defined as

$$z_k = \frac{x_e(k) - \bar{s}_{k-1}}{\sigma_{s_{k-1}}}. \tag{43}$$

Table 2
Parameter setting and initialization.

Parameter	Value	Parameter	Value
$e(0)$	$[0,\ 0]^{\mathrm{T}}$	$\hat{e}(0)$	$[0,\ 0]^{\mathrm{T}}$
$\overline{d}_a(0)$	0	$\hat{\overline{d}}_a(0)$	0
ξ	0.8	ω_n	0.05
K	0.5462	T	201.4375
α_3	30	v_{th}	3.5
l	15	i_n	0.8

Based on the Z-score z_k, the peak (mutation) detection of residual states can be performed, and the detection criterion is

$$Y_{t_k} = \begin{cases} 1, & x_e(k) < L_- \ or \ x_e(k) > L_+, \\ 0, & else, \end{cases} \tag{44}$$

where v_{th} is a constant; $L_+ = \bar{s}_{k-1} + v_{th}\sigma_{s_{k-1}}$ and $L_- = \bar{s}_{k-1} - v_{th}\sigma_{s_{k-1}}$ are the upper and lower bounds of the confidence interval, respectively.

When a mutation of the residual state is detected by the detection criterion at the kth sampling time, i.e., the steering machine fault occurs at $t_k = kt_s$, then the switching signal can be defined as

$$S_W(t) = \begin{cases} 1, & t \geq t_k, Y_{t_k} = 1, \\ 0, & else. \end{cases} \tag{45}$$

Based on the switching signal S_W, the switching controller can be described as

$$\begin{cases} L & = (1 - S_W(t))L_{i1} + S_W(t)L_{i2}, \\ u(t) & = (1 - S_W(t))\sum_{i=1}^r h_i(x(t))[K_{i1}\hat{e}(t)] \\ & \quad + S_W(t)\sum_{i=1}^r h_i(x(t))[K_{i2}\hat{e}(t) - \hat{\overline{d}}_a(t)]. \end{cases} \tag{46}$$

Remark 9. Combining Equations (44) and (45), it can be seen that once the mutation is detected, the alarm will generate the switching signal until the new mutation is detected.

Remark 10. To the best of the authors' knowledge, the smoothed Z-score algorithm was developed primarily for robust and adaptive peak (mutation point) detection of real-time signals [41–43]. Considering that the residual state will mutate immediately after the fault occurs. Consequently, it is feasible to use the smoothed Z-score algorithm for mutation detection and give the conclusion that the system is suffering from steering machine fault. Moreover, residuals are analyzed for fault detection and alarming, which helps to make the fault more intuitive.

4. Simulation experiment results

4.1. Experiment setup and preparation

In this part, the switching control is simulated by MATLAB, considering the "Yulong" ship investigated by Zhang and Jin [44]. The length L, width W, full load draught d, and block coefficient C_b of the ship are L = 126 m, W = 20.8 m, d = 8.0 m and $C_b = 0.681$, respectively. The nonlinear Norrbin model, reference model, and controller have the following parameters at forward speed of $v = 8.682$ m/s that are listed in Table 2.

We have utilized a nine-rule fuzzy model to describe the NSA system. And the system matrices A_i, B_i, C_i, and D_i for ith rule can be calculated according to the recent literature [45]. The fuzzy rules and their corresponding system matrices are listed in Appendix A.

For simplicity, the triangular membership functions shown in Fig. 6 are employed to describe the fuzzy sets of $x_1(t)$ and $x_2(t)$, respectively.

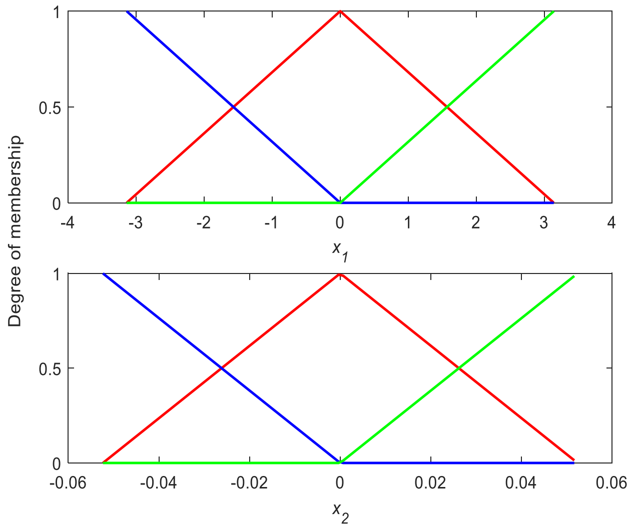

Fig. 6. Membership functions.

Next, based on Theorem 1 and Theorem 3, the following observer gain matrix L_{i1} and controller gain matrix K_{i1} in fault-free situations can be obtained. Similarly, L_{i2} and K_{i2} in faulty situations can be obtained as well based on Theorem 2 and Theorem 4. The results are exhibited in Appendix B.

4.2. Performance evaluation for the proposed switching control scheme

In this work, the system model (7) is used to approximate the actual NSA system. That is, the system model (7) is used to instead of the "real" ship. And two cases of simulation experiments are conducted to evaluate the performance of the proposed switching control scheme using the system model (7). It should be noted that the same command heading and external disturbance signals are used for the two cases. And the command heading and the external disturbances are employed as

$$\psi_r(t) = \begin{cases} 30^\circ & t \le 300 \\ 10^\circ & 300 < t \le 600 \\ 20^\circ & t > 600 \end{cases},$$

$$\omega(t) = \begin{cases} 5\sin(3\pi t), & t \le 900 \\ 0, & t > 900 \end{cases}.$$

Case 1: *Course tracking control in fault-free situations*

In Case 1, assuming that the NSA system is in fault-free situations, i.e., $\bar{d}_a(t) = 0$. At this time, there will be no fault alarm signal generated and only the robust controller K_{i1} is invoked. The results of actual heading tracking and its corresponding state response, residual analysis, and fault alarm signal are given in Fig. 7.

In Fig. 7(c), the residual analysis, the detection result Y, and the fault alarm signal S_W are given. Where Y denotes the detection result of the residual state mutation and S_W is the switching signal generated based on the detection result Y. From the results of the residual analysis, it can be seen that the residual values will always be located between the upper and lower bounds of the confidence interval without generating Y and S_W in fault-free situations. In this case, observer L_{i1} and controller K_{i1} are used to enable the state estimation and control of the NSA system. Specifically, observer L_{i1} is invoked and used to estimate the system state, and controller K_{i1} is invoked and used to control the ship traveling on the desired heading effectively. As can be seen from Fig. 7, controller K_{i1} can control the ship traveling on the desired heading effectively in fault-free situations. And it can be seen from Fig. 7(b) that the observer L_{i1} designed in this paper enables the accurate estimation of the system state. Also, by analyzing the system residual signal in real-time (Fig. 7(c)), the effective monitoring of system status is realized.

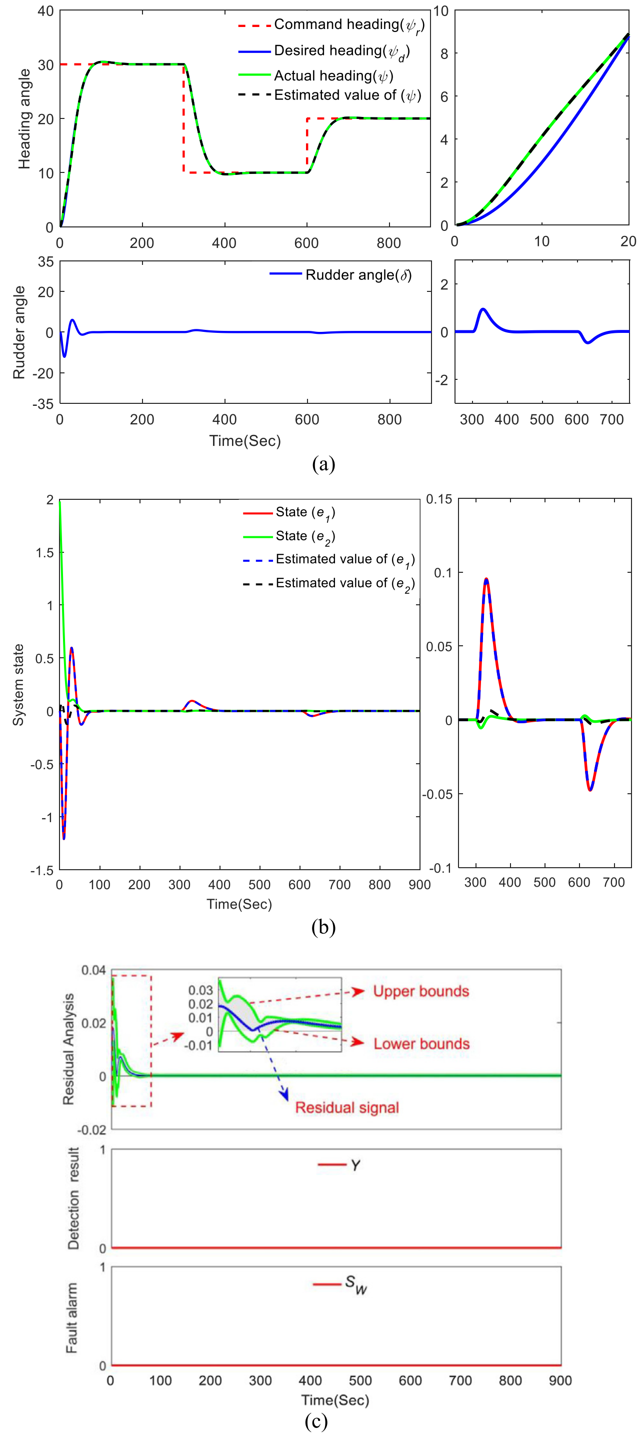

Fig. 7. Simulation results for Case 1. (a) Command heading ψ_r, desired heading ψ_d, actual heading ψ, estimated value of ψ, and rudder angle δ. (b) System states (e_1, e_2) and their estimations. (c) Residual analysis, detection result Y, and fault alarm signal S_W.

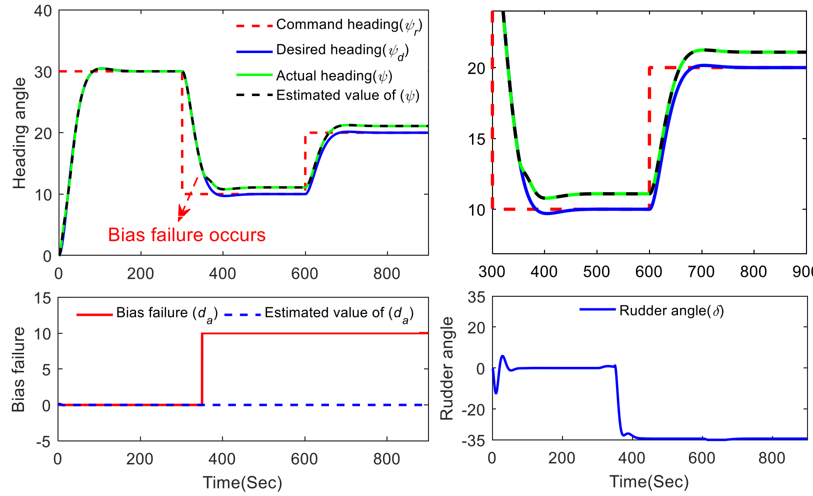

(a)

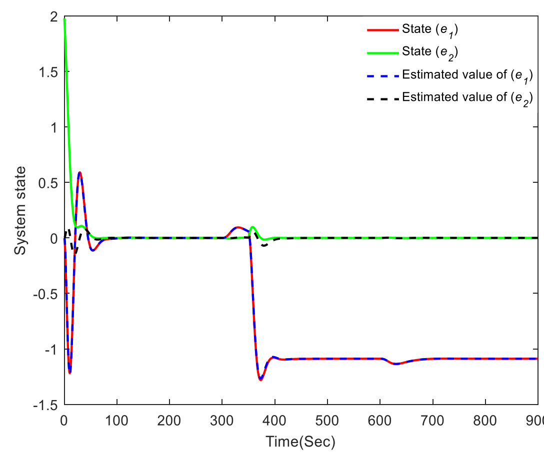

(b)

Fig. 8. Simulation results for Case 2. (a) Command heading ψ_r, desired heading ψ_d, actual heading ψ, estimated value of ψ, bias failure $\overline{d}_a$, estimated value of $\overline{d}_a$, and rudder angle δ. (b) System states (e_1, e_2) and their estimations.

Case 2: *Course tracking control in faulty situations*

In Case 2, the NSA system control in faulty situations is considered, i.e., $\overline{d}_a(t) = 10+exp(-0.2*t), t \geq 350$. In this case, the NSA system fails to be effectively controlled if the pre-fault controller K_{i1} continues to be used. The simulation results are given in Fig. 8.

From Fig. 8, we can see that the continued use of controller K_{i1} will cause the system states e_1 and e_2 to diverge, and deviate the ship from its desired heading in faulty situations. The reason for such deviations is that the observer L_{i1} cannot realize the real-time estimation of the fault information $\overline{d}_a$ to compensate for the faulty system.

In faulty situations, with the switching control scheme designed in this paper, the fault alarm operates and generates the switching signal S_W, and K_{i2} is called. The simulation results of switching control for ship course tracking based on fault alarm signal are given in Fig. 9.

From Fig. 9(c), the mutation of the residual state occurs at $t \geq 350$, and the residual value exceeds the upper bound of the confidence interval L_+. Then, it is capable for FDA to detect the mutation of the residual state in time and give the detection result Y. Meanwhile, based on the detection result Y, the fault signal S_W will be generated. It can be seen that the FDA is able to achieve effective detection of steering machine fault by analyzing the system residual signal in real-time and S_W will be given in faulty (bias fault) situations. At this time, based on the switching signal S_W, the NSA system will switch to the fault-tolerant controller K_{i2} and the faulty system will be compensated by using the fault information $\widehat{\overline{d}}_a$ estimated by the observer L_{i2} in real-time. Then, the stability of system is ensured.

Remark 11. Comparing Figs. 8 and 9, it can be easily seen that timely and effective detection of fault information and switching to the suitable controller based on alarm signals ensures the stable operation of NSA system in faulty situations. It is meaningful for the stability control research of actual systems.

Remark 12. In this remark, the detailed analysis of the switching mechanism is presented in conjunction with Figs. 8 and 9. Specifically, L_{i1} and K_{i1} are used to ensure stable control of the NSA system when $t < 350$, i.e., the system is in fault-free situations. From Fig. 9(c), it can be seen that the FDA does not generate the switching signal S_W in this case, which is consistent with the actual situation. When $t \geq 350$, the actuator bias fault occurs, which results in the system state divergence and the NSA system cannot be effectively controlled if the controller K_{i1} is adopted continuously (Fig. 8). In faulty situations, the FDA generates a valid switching signal S_W, and L_{i2} and K_{i2} are invoked and used to ensure the stable control of the NSA system. Meanwhile, the

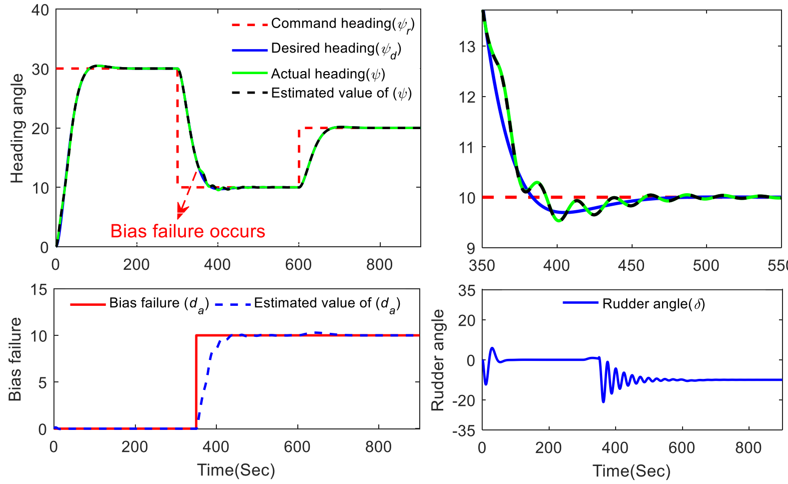

(a)

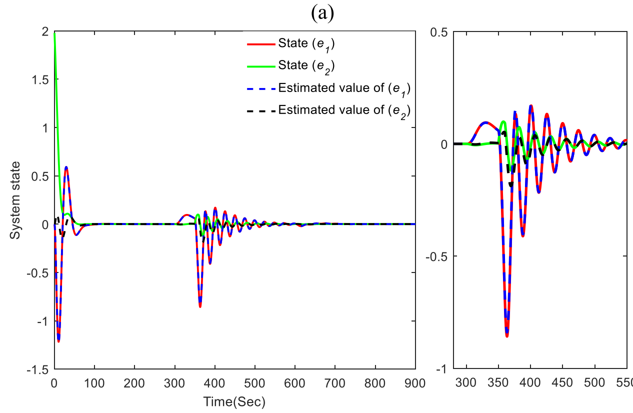

(b)

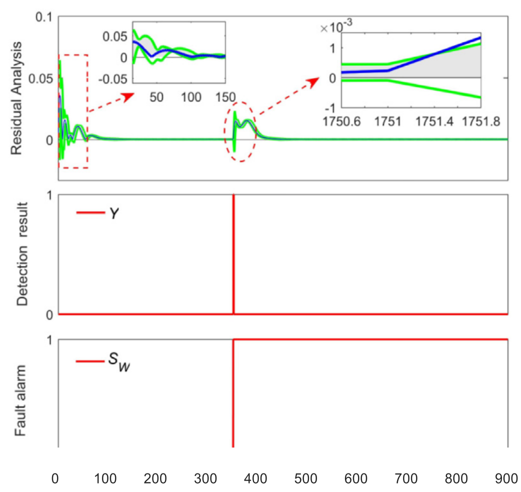

(c)

Fig. 9. Simulation results for Case 2. (a) Command heading ψ_r, desired heading ψ_d, actual heading ψ, estimated value of ψ, bias failure $\overline{d}_a$, estimated value of $\overline{d}_a$, and rudder angle δ. (b) System states (e_1, e_2) and their estimations. (c) Residual analysis, detection result Y, and fault alarm signal S_W.

system state and heading error converged gradually (Fig. 9(a) and (b)), and the NSA system will be controlled effectively.

5. Conclusions

In this work, the issue of fault-tolerant control for NSA is investigated. A fault-tolerant switching control system is designed for ship course tracking with integrated VFOs, VFO-HRC, VFO-HFTC, and FDA. The proposed method for mitigating the effects of steering machine fault is an active fault-tolerant control scheme implemented by switching. VFOs are introduced to estimate the system state and unknown bias fault simultaneously, and the VFO-HRC and VFO-HFTC are designed for fault-free and faulty systems, respectively. Moreover, the FDA is developed to detect faults promptly and efficiently, and the NSA system is provided with an alarm signal to invoke the appropriate controller and corresponding observer. Furthermore, simulations are conducted to demonstrate the effectiveness of the developed control method.

In summary, the switching control with VFO-HRC, VFO-HFTC, and FDA proposed in this paper provides an effective heading control scheme for course tracking and reduces the conservativeness of the system, which can be used as a theoretical reference for high-performance control of NSA system. This switching control method is applicable to a class of nonlinear systems with actuator faults and immeasurable states. Furthermore, this method facilitates the reduction of sensor costs and is suitable for NSA systems equipped with low-cost sensors, which provides good practical value in real engineering. Currently, the fault-tolerant control of NSA system mitigates the effect of steering machine fault by switching. In future work, a fuzzy adaptive course tracking control method will be further investigated to reduce the impact of frequent switching actions on the performance and stability of the system.

Declaration of competing interest

The authors declare that they have no known competing financial interests or personal relationships that could have appeared to influence the work reported in this paper.

Acknowledgments

We acknowledge financial support from the National key R&D projects, China (2022YFE0210700), the Zhejiang Provincial Natural Science Foundation of China (No. LZ22F030008), the Zhejiang Province Key R&D projects, China (No. 2021C03015), the Zhejiang Province Outstanding Youth Fund (LR21F030001), the NSFC, China (No. 52171352), the Fundamental Research Funds for the Provincial Universities of Zhejiang, China (GK229909299001-012), the National Natural Science Foundation of China (No. 61733009).

Appendix A

The fuzzy rules are listed as follows:

R₁: IF $x_1(t)$ is about $-\pi$ and $x_2(t)$ is about $-\pi/60$,
THEN $\dot{e}(t) = A_1 e(t) + B_1 u(t) + D_1 \varpi(t), y(t) = C_1 e(t) + \psi_d$,

R₂: IF $x_1(t)$ is about $-\pi$ and $x_2(t)$ is about 0,
THEN $\dot{e}(t) = A_2 e(t) + B_2 u(t) + D_2 \varpi(t), y(t) = C_2 e(t) + \psi_d$,

R₃: IF $x_1(t)$ is about $-\pi$ and $x_2(t)$ is about $\pi/60$,
THEN $\dot{e}(t) = A_3 e(t) + B_3 u(t) + D_3 \varpi(t), y(t) = C_3 e(t) + \psi_d$,

R₄: IF $x_1(t)$ is about 0 and $x_2(t)$ is about $-\pi/60$,
THEN $\dot{e}(t) = A_4 e(t) + B_4 u(t) + D_4 \varpi(t), y(t) = C_4 e(t) + \psi_d$,

R₅: IF $x_1(t)$ is about 0 and $x_2(t)$ is about 0,
THEN $\dot{e}(t) = A_5 e(t) + B_5 u(t) + D_5 \varpi(t), y(t) = C_5 e(t) + \psi_d$,

R₆: IF $x_1(t)$ is about 0 and $x_2(t)$ is about $\pi/60$,
THEN $\dot{e}(t) = A_6 e(t) + B_6 u(t) + D_6 \varpi(t), y(t) = C_6 e(t) + \psi_d$,

R₇: IF $x_1(t)$ is about π and $x_2(t)$ is about $-\pi/60$,
THEN $\dot{e}(t) = A_7 e(t) + B_7 u(t) + D_7 \varpi(t), y(t) = C_7 e(t) + \psi_d$,

R₈: IF $x_1(t)$ is about π and $x_2(t)$ is about 0,
THEN $\dot{e}(t) = A_8 e(t) + B_8 u(t) + D_8 \varpi(t), y(t) = C_8 e(t) + \psi_d$,

R₉: IF $x_1(t)$ is about π and $x_2(t)$ is about $\pi/60$,
THEN $\dot{e}(t) = A_9 e(t) + B_9 u(t) + D_9 \varpi(t), y(t) = C_9 e(t) + \psi_d$,

where $A_1 = \begin{bmatrix} 0 & -1 \\ 0 & -0.0062 \end{bmatrix}$, $A_2 = \begin{bmatrix} 0 & -1 \\ 0 & -0.0054 \end{bmatrix}$, $A_3 = \begin{bmatrix} 0 & -1 \\ -1.36 \times 10^{-5} & -0.0062 \end{bmatrix}$, $A_4 = \begin{bmatrix} 0 & -1 \\ 0 & -0.0054 \end{bmatrix}$, $A_5 = \begin{bmatrix} 0 & -1 \\ 0 & -0.0050 \end{bmatrix}$, $A_6 = \begin{bmatrix} 0 & -1 \\ 0 & -0.0054 \end{bmatrix}$, $A_7 = \begin{bmatrix} 0 & -1 \\ -1.36 \times 10^{-5} & -0.0062 \end{bmatrix}$, $A_8 = \begin{bmatrix} 0 & -1 \\ 0 & -0.0050 \end{bmatrix}$, $A_9 = \begin{bmatrix} 0 & -1 \\ -1.36 \times 10^{-5} & -0.0062 \end{bmatrix}$, $B_1 = B_2 = \cdots = B_9 = [00.0027]^{\mathrm{T}}$, $C_1 = C_2 = \cdots = C_9 = [-10]$,

$D_1 = D_2 = \cdots = D_9 = \begin{bmatrix} 1 & 0 \\ 0 & -0.0050 \end{bmatrix}$.

Appendix B

Let the H_∞ performance γ of the observer L_{i1} and the controller K_{i1} is $\gamma = 1.2$, then the observer gain matrix L_{i1} and controller gain matrix K_{i1} in fault-free situations are as follows:

$L_{11} = [-26.2574\ 0.4976]^{\mathrm{T}}, L_{21} = [-25.8499\ 0.6727]^{\mathrm{T}}$,
$L_{31} = [-26.4612\ 0.4731]^{\mathrm{T}}$,

$L_{41} = [-12.9742\ 1.7073]^{\mathrm{T}}, L_{51} = [-5.41378\ 1.3362]^{\mathrm{T}}$,
$L_{61} = [-7.2436\ 2.1414]^{\mathrm{T}}$,

$L_{71} = [-12.9098\ 1.6093]^{\mathrm{T}}, L_{81} = [-7.1871\ 2.1363]^{\mathrm{T}}$,
$L_{91} = [-13.1238\ 1.6149]^{\mathrm{T}}$,

$K_{11} = [10.0708\ -2.6640], K_{21} = [9.1916\ -2.5161]$,
$K_{31} = [10.3855\ -2.7181]$,

$K_{41} = [8.7259\ -2.4403], K_{51} = [9.1889\ -2.5101]$,
$K_{61} = [8.0643\ -2.3375]$,

$K_{71} = [8.6343\ -2.4251], K_{81} = [7.9407\ -2.3194]$,
$K_{91} = [9.0915\ -2.4996]$.

Let the H_∞ performance $\overline{\gamma}$ of the observer L_{i2} and the controller K_{i2} is $\overline{\gamma} = 2.8$, then the observer gain matrix L_{i2} and controller gain matrix K_{i2} in fault-free situations are as follows:

$L_{12} = [-3.2031\ 0.7416\ 16.0565]^{\mathrm{T}}$,
$L_{22} = [-3.4560\ 0.7956\ 17.1123]^{\mathrm{T}}$,

$L_{32} = [-3.2846\ 0.7595\ 16.4448]^{\mathrm{T}}$,
$L_{42} = [-3.4718\ 0.8469\ 18.1700]^{\mathrm{T}}$,

$L_{52} = [-3.4799\ 0.8170\ 17.5420]^{\mathrm{T}}$,
$L_{62} = [-3.2799\ 0.7354\ 15.8992]^{\mathrm{T}}$,

$L_{72} = [-3.2943\ 0.8115\ 17.4611]^{\mathrm{T}}$,
$L_{82} = [-3.4322\ 0.7751\ 16.7013]^{\mathrm{T}}$,

$L_{92} = [-3.2554\ 0.7804\ 16.8361]^{\mathrm{T}}$,

$K_{12} = [22.4329\ -9.9662], K_{22} = [19.8668\ -8.8810]$,
$K_{32} = [20.0207\ -8.9559]$,

$K_{42} = [20.5542\ -10.4104], K_{52} = [23.0011\ -11.5994]$,
$K_{62} = [22.8319\ -10.0959]$,

$K_{72} = [21.3347\ -9.5262], K_{82} = [24.7048\ -12.2991]$,
$K_{92} = [21.4089\ -9.5051]$.

References

[1] Ejaz M, Chen M. Sliding mode control design of a ship steering autopilot with input saturation. Int J Adv Robot Syst 2017;14(3):1–13.
[2] Minorsky N. Directional stability of automatically steered bodies. Nav Eng J 2009;34(2):280–309.
[3] Öztürk Ü, Boz HA, Balcisoy S. Visual analytic based ship collision probability modeling for ship navigation safety. Expert Syst Appl 2021;175:114755.
[4] Banerjee A, Mukherjee J, Nabi MU, Kar IN. An artificial delay based robust guidance strategy for an interceptor with input saturation. ISA Trans 2020;109:34–48.
[5] Lee SD, Yu CH, Hsiu KY, Hsieh YF, Tzeng CY, Kehr YZ. Design and experiment of a small boat track-keeping autopilot. Ocean Eng 2010;37(2–3):208–17.
[6] Li Z, Sun J. Disturbance compensating model predictive control with application to ship heading control. IEEE Trans Control Syst Technol 2012;20(1):257–65.
[7] Banazaden A, Ghorbani MT. Frequency domain identification of the nomoto model to facilitate Kalman filter estimation and PID heading control of a patrol vessel. Ocean Eng 2013;72:344–55.
[8] Xu H, Soares CG. Vector field path following for surface marine vessel and parameter identification based on LS-SVM. Ocean Eng 2016;113:151–61.
[9] Zhang J, Sun T, Liu Z. Robust model predictive control for path following of under actuated surface vessels with roll constraints. Ocean Eng 2017;143:125–32.
[10] Perera LP, Soares CG. Lyapunov and hurwitz based controls for input–output linearization applied to nonlinear vessel steering. Ocean Eng 2013;66:58–68.
[11] Du J, Hu X, Sun Y. Adaptive robust nonlinear control design for course tracking of ships subject to external disturbances and input saturation. IEEE Trans Syst Man Cybern 2020;50(1):193–202.
[12] Liu Z, Chu R. Robust adaptive heading control for a surface vessel with drift angles. Ocean Eng 2020;205:1–8.
[13] Liu Z. Adaptive extended state observer based heading control for surface ships associated with sideslip compensation. Appl Ocean Res 2021;110:102605.
[14] Zhang XK, Zhang GQ. Design of ship course-keeping autopilot using a sine function based nonlinear feedback technique. J Navig 2016;69(2):246–56.
[15] Zhang XK, Zhang GQ, Chen XJ. A novel nonlinear feedback control and its application to course-keeping autopilot. J Mar Sci Tech 2016;24(2):192–8.
[16] Zhang XK, Zhang GQ. Determining robust parameters in stabilizing set of backstepping based nonlinear controller for ships' course keeping. Int J Marit Eng 2016;158(4):269–73.
[17] Zhang XK, Yang G, Zhang Q, Zhang G, Zhang Y. Improved concise backstepping control of course keeping for ship using nonlinear feedback technique. J Navig 2017;70(6):1401–14.
[18] Zhang XK, Zhang Q, Ren HX, Yang GP. Linear reduction of backstepping algorithm based on nonlinear decoration for ship course-keeping control system. Ocean Eng 2018;147:1–8.
[19] Yang Y, Zhou C, Ren J. Model reference adaptive robust fuzzy control for ship steering autopilot with uncertain nonlinear systems. Appl Soft Comput 2003;3:305–16.
[20] Yang Y, Ren J. Adaptive fuzzy robust tracking controller design via small gain approach and its application. IEEE Trans Fuzzy Syst 2003;11:783–95.
[21] Yang YS. Robust control of uncertain systems and its applications. Beijing: Science Press; 2004.
[22] Yang Y, Zhou C. Adaptive fuzzy control of ship autopilots with uncertain nonlinear systems. IEEE Conf Cybern Intell Syst 2004;2:1323–8.
[23] Omerdic E, Roberts GN, Vukic Z. Reconfigurable control for ship steering. Proc Inst Mech Eng 2003;217(1):25–39.
[24] Cheng XQ, Qu JY, Yan ZP, Bian XQ. H_∞ Robust fault-tolerant controller design for autonomous underwater vehicle's navigation control system. J Mar Sci Appl 2010;9(1):87–92.
[25] Zheng Y, Liu Z, Liu L. Robust MPC-based fault-tolerant control for trajectory tracking of surface vessel. IEEE Access 2018;6(1):14755–63.
[26] Fossen TI. Marine control systems. Trondheim, Norway: Marine Cybernetics; 2002.
[27] Fan Y, Mu D, Zhang X, Wang G, Guo C. Course keeping control based on integrated nonlinear feedback for a USV with pod-like propulsion. J Navig 2018;71(4):878–98.
[28] Mark MM. Mathematical modeling. Beijing: China Machine Press; 2005.
[29] Zhang X, Xu X, Li J, Ma F, Chen Y, Xu X, et al. A novel switching control for ship course-keeping autopilot with steering machine bias failure and fault alarm. Ocean Eng 2022;261:112191.
[30] Li X, Xu QA, Blaabjerg F. Adaptive resilient secondary control for islanded ac microgrids with sensor faults. IEEE J Em Sel Top 2020;9:5239–48.
[31] Lee TH, Lim CP, Nahavandi S, Roberts RG. Observer-based H_∞ fault-tolerant control for linear systems with sensor and actuator faults. IEEE Syst J 2019;13:1981–90.
[32] Huang M, Ding L, Li W, Chen C, Liu Z. Distributed observer-based H_∞ fault-tolerant control for dc microgrids with sensor fault. IEEE T Circuits-I 2021;68:1659–70.
[33] Fossen TI. Guidance and control of ocean vehicles. New York, the United States: John Wiley & Sons Inc; 1994.
[34] Zhang K, Jiang B, Staroswiecki M. Dynamic output feedback fault tolerant controller design for Takagi–Sugeno fuzzy systems with actuator faults. IEEE Trans Fuzzy Syst 2010;18(1):194–201.
[35] Huang SJ, Yang GH. Fault tolerant controller design for T-S fuzzy systems with time-varying delay and actuator faults: A k-step-faultestimation approach. IEEE Trans Fuzzy Syst 2014;22(6):1526–40.
[36] Lin C, Wang QG, Lee TH, He Y, Chen B. Observer-based H_∞ control for t-s fuzzy systems with time-delay: delay-dependent design method. IEEE Trans Syst Man Cybern B 2007;37(4):1030–8.
[37] Zhao XQ, Guo S, Long Y, Zhong GX. Simultaneous fault detection and control for discrete-time switched systems under relaxed persistent dwell time switching. Appl Math Comput 2022;412:1–16.
[38] Li JN, Wang A, Miao K, Li L. Failure-distribution-dependent H_∞ fuzzy fault-tolerant control for multiple-degree-of-freedom nonlinear bilateral teleoperation system. J Frankl Inst 2020;357:13511–33.
[39] Zhang D, Wang QG, Yu L, Shao QK. Filtering for networked systems with multiple time-varying transmissions and random packet dropouts. IEEE Trans Ind Inform 2013;9(3):1705–16.
[40] Koh BH, Li Z, Dharap P, Nagarajaiah S, Phan MQ. Actuator failure detection through interaction matrix formulation. J Guid Control Dyn 2005;28:895–901.
[41] Catalbas MC, Cegovnik T, Sodnik J, Gulten A. Driver fatigue detection based on saccadic eye movements. In: 10th International conference on electrical and electronics engineering. ELECO, 2017, p. 913–7.
[42] Perkins P, Heber S. Identification of ribosome pause sites using a z-score based peak detection algorithm. In: IEEE 8th international conference on computational advances in bio and medical sciences. ICCABS, 2018, p. 1–6.
[43] Lima BMR, Ramos LCS, Oliveira TEA, Fonseca VP, Petriu EM. Heart rate detection using a multimodal tactile sensor and a z-score based peak detection algorithm. In: CMBES proceedings. 2019, p. 42.
[44] Zhang XK, Jin YC. Transfigured loop shaping controller and its application to underwater vehicle. Int J Autom Comput 2005;2(1):48–51.
[45] Liu JK, Liu ZJ. Control system design analysis and matlab simulation based on LMI. Beijing: Tsinghua University Press; 2020.